https://doi.org/10.5194/egusphere-2025-1578
Preprint. Discussion started: 16 April 2025

Amplified Warming and Marine Heatwaves in the North Sea Under a Warming Climate

Bayoumy Mohamed[1,2,*], Alexander Barth[1], Dimitry Van der Zande[3], and Aida Alvera-Azcárate[1]

[1]GeoHydrodynamics and Environment Research (GHER), University of Liège, Liège, Belgium
[2] Oceanography Department, Faculty of Science, Alexandria University, Alexandria 21500, Egypt
[3] Operational Directorate Natural Environment, Royal Belgian Institute of Natural Sciences, Brussels, Belgium

* *Correspondence to: Bayoumy Mohamed (*bayoumy.mohamed@uliege.be*)*

Abstract: The Northeast Atlantic and adjacent regions, such as the North Sea, are among the fastest-warming areas in the world. However, the role of climate change and internal variability on marine heatwaves (MHWs) in this region remains poorly understood. This study aims to quantify the relevant changes in sea surface temperature (SST) and MHWs in the North Sea, as well as to identify the leading patterns of interannual MHW variability over more than four decades (1982–2024). Our results indicate a new regime shift in the annual mean SST in the North Sea since 2013. Therefore, we examine the relationships between MHW trends and long-term SST warming trends to quantify the role of climate change in the intensification of MHWs. We found that the increase in MHWs is related to the significant decadal change in SST over the North Sea, and we have revealed that large-scale climate modes, such as the Atlantic Multidecadal Oscillation and the East Atlantic Pattern, play a crucial role in this decadal change in SST. In particular, the SST trend has doubled in recent years (post-2013) compared to the previous period (1982–2012: pre-2013), leading to more intense and frequent MHWs. The SST and MHW frequencies have significantly increased by 0.38°C/decade and 1.04 events/decade, respectively, over the entire study period. After removing the long-term SST warming trend before MHW detection, all MHW features exhibited insignificant trends, indicating that the long-term SST trend is the primary driver of the observed long-term MHW trend in the North Sea region, thereby confirming the crucial role of mean SST changes in MHW in this region. Furthermore, we found that 80% of the observed trend in MHW frequency is attributed to long-term warming, while the rest is attributed to internal variability. The SST record in May 2024, manifested by the longest (27 days) and most intense (2.2°C) MHW event, is attributed to an anomalous anticyclonic atmospheric circulation over the Baltic Sea and southern Norway, which enhances solar radiation over the North Sea. Finally, our results showed an opposite response of chlorophyll-a concentrations to MHWs, with an increase in the coastal areas of the southern part and a decrease in the northeastern part of the North Sea.

Keywords: Extreme SST events, Intensifying Marine Heatwaves, North Sea Warming, Chlorophyll-a, Climate Change. Regime shift.

1. Introduction

With anthropogenic global warming, extreme sea surface temperature (SST) events such as marine heatwaves (MHWs) have increased worldwide, posing a challenge for scientific research and public policy (IPCC 2021). However, the increase in these events is neither temporally nor spatially uniform but varies depending on the period and geographical region under consideration. Quantifying these extreme events and assessing their key drivers and impacts has been one of the biggest challenges for climate research in recent years. The changes caused by climate change and the escalation of these extreme

https://doi.org/10.5194/egusphere-2025-1578
Preprint. Discussion started: 16 April 2025

events are closely linked to human activities. These extreme events exacerbate thermal stress for marine organisms even more than shifts in mean climate conditions (Harris et al., 2018; Villeneuve and White, 2024). Researchers show that prolonged MHW events significantly impact aquatic ecosystems and fisheries and subsequently affect human life (Harris et al., 2018; Villeneuve and White, 2024). MHWs have been documented in the world's oceans from the Arctic to the Antarctic oceans and in the marginal Seas (Pecuchet et al., 2025). They occur both on the surface and in the subsurface and can extend to the sea floor.

Recent studies have reported a significant increase in the frequency, intensity, and duration of MHW in the Northeast Atlantic (Berthou et al., 2024; Jacobs et al., 2024; Simon et al., 2023a), and in the North Sea (Chen et al., 2022; Mohamed et al., 2023). Generally, MHWs in these shallow water regions are more sensitive to regional and local atmospheric processes (e.g., increased solar radiation, lower winds and cloud cover, and tropical air). For the southern North Sea, the causal factors for the MHW have been linked to atmospheric circulation patterns and the interannual variability of climate modes such as the Atlantic Multidecadal Oscillation (AMO), the North Atlantic Oscillation (NAO), and the East Atlantic Pattern (EAP). On the interannual time scale, the positive phases of the AMO and the EAP favor the development of a strong MHW, while the NAO makes the largest contribution only in winter (Mohamed et al., 2023). In other studies, the variability of MHW in the southern North Sea has been attributed to changes in stratification, suggesting an important role in the vertical structure of the ocean (Chen et al., 2022).

In this study, we focus on the North Sea (Fig. 1A), a shallow, semi-enclosed northwestern European shelf sea with openings to the Atlantic Ocean in the north (Norwegian Sea) and in the south (English Channel), which is connected to the Baltic Sea in the east by the Skaggerak Strait. The North Sea is strongly influenced by warm Atlantic Water inflow from the northern and southern openings and freshwater from the Baltic Sea. The North Sea hosts large commercial fish populations and is considered one of the most productive fisheries in Europe, and a major marine ecosystem (Alvera-Azcárate et al., 2021; Ducrotoy et al., 2000). Therefore, climate change and extreme events in this region could have a profound impact on the biological systems (Kirby et al., 2007).

In the northeast Atlantic and adjacent regions such as the Bay of Biscay, the Celtic Sea, the English Channel, and the North Sea, a regime shift occurred at the end of the last century (1990s) (Alheit et al., 2019; Biguino et al., 2023) . This shift was caused by complex ocean-atmosphere interactions that led to large-scale changes in the strength and direction of the current systems that move the water masses in the North Atlantic and caused a decline in the Atlantic Meridional Overturning Circulation (AMOC) (Marzocchi et al., 2015) . This climate shift was also accompanied by a significant weakening of the NAO (Robson et al., 2012) and a strong increase in the AMO (Biguino et al., 2023; Hughes et al., 2012). More than 25 years have passed since this regime shift (Fig. 1A) in the North Sea. Our research suggests that a new shift has recently occurred in the North Sea (Fig. 1B). A broad application of climate variability and prediction related to these regime shifts would be possible. For example, these are crucial for understanding the dynamics that amplify regional MHWs.

Our overarching goal in this study is to quantify the role of climate change and internal variability in the occurrence of MHW in the North Sea over more than four decades (1982–2024). Therefore, we focus on the following questions. (1) Has there been a recent new shift in the SST regime in the North Sea? (2) How does the change in mean SST explain the trends in MHW characteristics? (3) What are the main causes of the strongest and most intense MHW in spring 2004? (4) What

https://doi.org/10.5194/egusphere-2025-1578
Preprint. Discussion started: 16 April 2025

are the anomalous responses of chlorophyll-a concentration (an indicator of phytoplankton biomass) to MHW during the overlap period with chlorophyll data (1998–2024)?

2. Materials and Methods

2.1 Dataset

In this study, we used the daily NOAA Optimum Interpolation Sea Surface Temperature Dataset version 2.1 [OISST, (Huang et al., 2021; Reynolds et al., 2007)]. This dataset covers the period from January 1982 to December 2024, with a spatial resolution of 0.25 degrees in both latitude and longitude. In addition, the atmospheric variables were extracted from the ERA-5 reanalysis products of the European Center for Medium-Range Weather Forecasts [ECMWF, (Hersbach et al., 2020)]. This dataset covers the same period and spatial resolution as the SST. From this product, we have used the daily mean surface air temperature (SAT, hereafter), the u- and v-components of the wind speed (measured at 10 m height), the mean sea level pressure (MSLP), and the geopotential height at 500 hPa, as well as the components of the heat budget (shortwave radiation, longwave radiation, latent heat flux, and sensible heat flux). The ERA5 data are used to analyze the anomalous synoptic pattern and weather conditions during the longest and most extreme 2024 MHW event. Furthermore, we also used a monthly time series of climate indices representing the EAP and AMO climate modes. These climate mode data were obtained from the NOAA Physical Sciences Laboratory website (https://psl.noaa.gov/gcos_wgsp/Timeseries/, accessed January 2025). Finally, we used the daily high-resolution (1 km) cloud-free chlorophyll-a concentrations from multi-satellites downloaded from the Atlantic Ocean Colour product (Copernicus-GlobColour Project, https://doi.org/10.48670/moi-00289, last accessed February 2025). We used this dataset to investigate the chlorophyll-a responses to MHW during the overlap period (1998–2024).

2.2 Methods

All statistical analyses in this study were performed using the MATLAB program R2021a. For the detection and analysis of MHWs, the Marine Heatwaves Toolbox (Zhao and Marin, 2019), which implements the definition of Hobday et al. (2016), was applied to the daily SST data for each grid cell in the North Sea to detect the MHWs characteristics. For the trend analyses, seasonality, significance tests, Empirical Orthogonal Functions (EOFs), and graphical output, we mainly used the Climate Data Toolbox (Greene et al., 2019). A linear trend analysis was performed to determine the long-term trends of both SST and MHW metrics (frequency, total number of days, and cumulative intensity). Then, the non-parametric Modified Mann–Kendall (MMK) test (Hamed and Ramachandra Rao, 1998; Wang et al., 2020) was used to determine whether the linear trends were significant at the 95% confidence level.

There are several well-documented methods for detecting regime shifts, which in modern climate change studies are defined as a rapid transition from one mean climate state to another (Rodionov, 2004; Zeileis et al., 2003). These methods are based on statistical hypothesis tests and can reproducibly identify regime shifts as significant abrupt changes in the SST time series. These methods can be used to test the significance of the occurrence of a single or multiple abrupt change points. Here, we employ the Pettitt homogeneity test (Pettitt, 1979), which is described in Biguino et al. (2023). The Pettitt test is a nonparametric test commonly used with hydrometeorological variables to determine the occurrence and timing of a single abrupt and significant change in the mean of a time series (Biguino et al., 2023). In addition, the cumulative deviation test (Rebstock, 2002) was applied to determine whether multiple change points were detected.

https://doi.org/10.5194/egusphere-2025-1578
Preprint. Discussion started: 16 April 2025

For the MHW calculations, we followed the methodology of Hobday et al. (2016), who define MHW when the SST at a given location is above the corresponding seasonally varying 90th percentile threshold for at least five consecutive days, based on a fixed reference baseline, here we used the period 1982–2024 as the baseline climatology. Furthermore, to assess the effect of long-term warming (i.e., mean climate change) and internal variability on MHWs, the linearly detrended SST from 1982 to 2024 was calculated at each grid point to detect MHWs. Then, MHWs were re-identified by calculating a new threshold using the detrended SST data and recalculating the corresponding MHW metrics (Lee et al., 2023). This approach is commonly referred to as one of the shifting baselines (Amaya et al., 2023).

Therefore, both a fixed and a linearly shifting baseline were used in our MHW calculations to isolate the effect of the long-term SST trend on the MHW metrics according to the following formula (Jin and Zhang, 2024; Lee et al., 2023; Simon et al., 2023b):

$$\text{MHW (SST}^{\text{trend}}) = \text{MHW (SST)}_{\text{fixed baseline}} - \text{MHW (SST}^{\text{detrended}})_{\text{shifting baseline}}$$

where MHW (SST) and MHW (SST $^{\text{detrended}}$) are the MHW metrics derived from the original SST time series (i.e., the contribution of both long-term warming and internal variability to MHW) and the detrended SST time series (i.e., the contribution of internal variability to MHW), respectively. The detrend method minimizes the impact of the increase in mean SST or long-term trend and analyzes the impact of changing SST variance. Moreover, we used the Trend Attribution Ratio (TAR) (Jin and Zhang, 2024; Li et al., 2023; Marin et al., 2021) to assess the relative contribution of the long-term SST trend and internal variability to the MHW trends:

$$\text{TAR} = \left(\frac{|rate^{trend}| - |rate^{detrend}|}{\max(|rate^{trend}|, |rate^{detrend}|)}\right)$$

Where, |---| is the absolute value of the trends, and rate $^{\text{trend}}$ and rate $^{\text{detrend}}$ are MHW trends attributed to the long-term SST trend and the internal SST variability, respectively. The TAR value ranges from −1 to 1. If the TAR value is close to 1 (−1), the long-term SST trend (internal variability) is the dominant driver of the observed MHW trend. When the TAR value is close to or equal to 0, the SST's long-term trend and internal variability contribute equally to the observed MHW trends.

In addition to the default MHW parameters proposed by Hobday et al. (2016) (e.g., frequency, total days, and cumulative intensity), we calculated the probability ratio (PR) and fraction of attributable risk (FAR) for each MHW based on Frölicher et al. (2018). The PR can be interpreted as a measure of how the number of MHW days has changed each year concerning the total record. The PR is estimated as P1/P0, where P1 is the probability of exceeding a relative threshold (90th percentile) in a year (i.e., the number of days exceeding the 90th percentile SST in a year/total number of days in that year). P0 is the probability of exceeding that threshold during the entire period (1982–2024) (i.e., the number of days on which the 90th percentile was exceeded during the whole period/total number of days during the entire period (15706 days). Thus, PR represents the relative strength of the MHW in each year compared to the totality of the records. It should be noted that the threshold for estimating PR for P0 is a constant, while for P1, it can change each year. If the PR is greater than 1, it indicates that the MHW change in that particular year exceeds the local threshold throughout the entire record (the corresponding risk will be higher), and vice versa if the PR is less than 1. This risk factor is known as the fraction of attributable risk (Frölicher et al., 2018). The FAR value for each year is calculated from the PR value as FAR = 1 – (1/PR). The FAR values vary from 0 to 1 (or 0%–100%) if PR $\geqslant$ 1. If PR < 1, which means that the MHW change is less than the local threshold,

https://doi.org/10.5194/egusphere-2025-1578
Preprint. Discussion started: 16 April 2025

the risk is zero. Finally, we associate the identified strongest and most intense MHW in spring 2024 with atmospheric factors on shorter time scales of a few days that are directly related to the intensification of this extreme event.

3. Results and Discussion

3.1 Regime shift and accelerated warming of the SST over the North Sea

To identify significant SST decadal changes, we analyzed the annual mean time series of SST over the North Sea. The horizontal distribution of the Pettitt test results is shown in Figure 1A. This non-parametric test allows us to determine the abrupt changing point in the SST time series that caused their heterogeneity (Biguino et al., 2023). Since this test reveals only a single change point in each time series (i.e., at each grid point), we applied it twice, first based on the entire study period (1982–2024), with the likely significant change point observed between 1996 and 2001 (Fig. 1A, top right panel). This period coincides with the AMO inversion from the negative to the positive phases (Mohamed and Skliris, 2025). This climate shift took place mainly over the southern and eastern parts of the North Sea in 1997 and over the northwestern part of the North Sea in 2001. This result is consistent with that found on the Iberian coast and in the Northeast Atlantic (Alheit et al., 2019; Biguino et al., 2023). As this regime shift is well documented for various subregions of the Northeast Atlantic, including the North Sea (Alheit et al., 2019), we then reapplied the Pettitt test for the second period following this shift (2001 to 2024) to investigate whether a new regime shift has recently occurred in the North Sea SST. Figure 1A (top left panel) shows that a significant new abrupt change in SST occurred mainly in 2013 over most of the North Sea, except for the northwestern part, where this shift occurred in 2009. The annual mean SST time series indicates this regime shift with a dominant positive SSTA after 2013. The SST has increased by 0.8°C from 2013 to 2024 (post-2013 period, hereafter) compared to 1982–2012 (pre-2013, hereafter). The second climate shift is associated with strong positive phases of the EAP during the post-2013 period.

For additional validation, the cumulative deviation test (Rebstock, 2002) is applied to corroborate a significant regime shift in the SST over the North Sea. The annual cumulative SSTA time series shows a prevalence of negative anomalies (i.e. decreasing tendency) until the first climate shift between 1996 and 2001, followed by a slight increase until 2013, while a prevalence of positive anomalies (i.e. increasing tendency) is observed in the post-2013 period (Fig. 1B). These changing tendencies indicate a significant climatic shift after 2013, with an increase in the mean and trend of SST compared to the pre-2013 period. The observed SST warming trend appears to be pronounced post-2013, with an estimated rate of 0.8°C/decade, compared to 0.4°C/decade during the pre-2013 period.

The regional mean of the daily SSTA time series was calculated by averaging the daily SSTA data of all grid cells in the North Sea throughout the entire study period (1982–2024) and plotted using a Hovmöller diagram (daily vs. annual), as shown in Figure 1C. There was a strong temporal development of the averaged SSTA, dividing our study period into three distinct periods. In the cold period (1982–1997), the negative SSTA dominates. This was followed by a transition period between 1998 and 2012, in which the SSTA fluctuated between negative and positive anomalies. During the period after 2013, the North Sea warmed dramatically and transitioned to a warmer state, with a sharp increase in SSTA and trend (Fig. 1C and Fig. 2).

https://doi.org/10.5194/egusphere-2025-1578
Preprint. Discussion started: 16 April 2025

Figure 2 shows the evolution of the monthly SSTA over time during the entire study period (1982–2024). The SSTA ranged from -1.8 to 1.6°C above the seasonal climatological baseline (1982–2024), with the lowest value recorded in 1986 and the highest in May 2024 (yellow star in Fig. 2, which will be explained in more detail in the following sections). Considering the approach of using monthly data instead of daily data to determine the MHW based on the fixed threshold (Capotondi et al., 2024), there are 52 warm events (yellow circles in Fig. 2) where the SSTA exceeds the fixed 90th percentile threshold (red dashed line in Fig. 2) and 50 marine cold spell events (MCS, green circles) where the SSTA is below the fixed 10th percentile threshold (blue dashed line). There is evidence of an increased frequency of warm events, with 32 warm events post-2013 compared to 20 warm events that occurred pre-2013 period. Most of the cold events occurred mainly before the first regime shift. The mean SSTA trend was estimated using the locally weighted scatterplot smoothing method (LOWESS; Cheng et al., 2022) and showed a rate of increase of 0.38°C/decade between 1982 and 2024, which also confirms the acceleration of warming after the crucial point of climate shift after 2013 (thick black line in Fig. 2). These results indicate that SST in the North Sea experienced two significant regime shifts in the late 1990s and after 2013. Therefore, in the next section, we focus on the most recent climate shift (post-2013) to investigate its role in amplifying MHW occurrence in the North Sea.

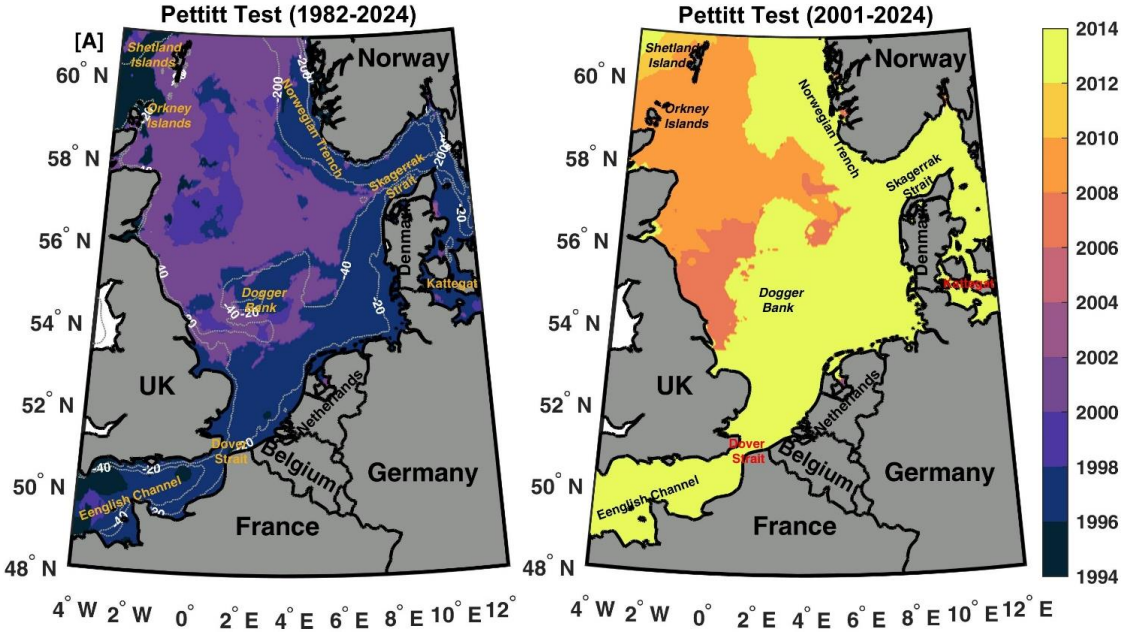

https://doi.org/10.5194/egusphere-2025-1578
Preprint. Discussion started: 16 April 2025

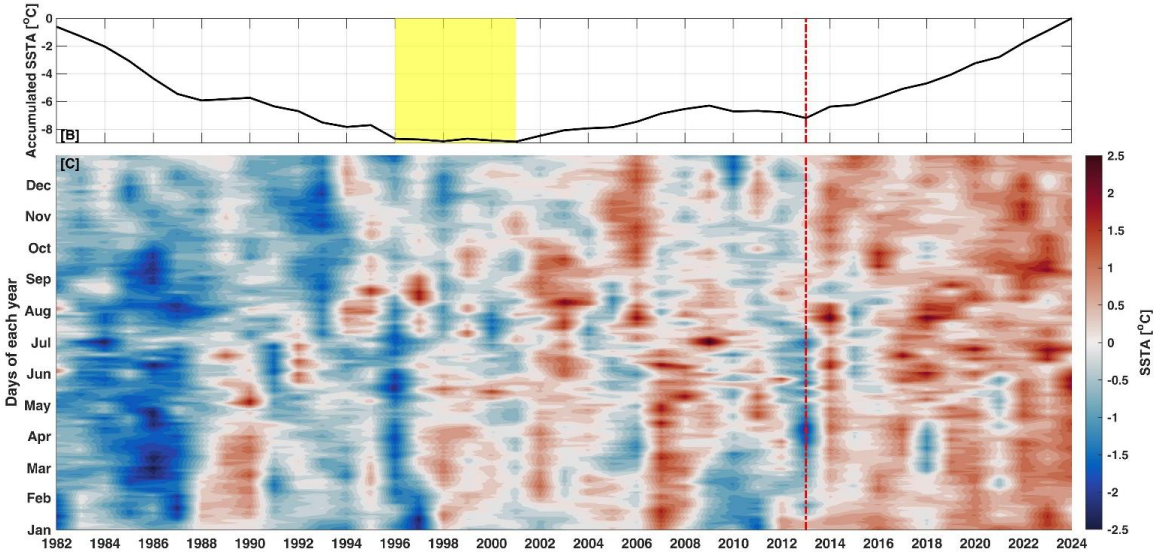

Figure 1: Regime shift of SST in the North Sea: (A) the horizontal distribution of significant change points (years) of the SST time series based on the Pettitt test during the whole period (1982–2024, top left) and in the last period (2001–2024, top right). (B) Long-term variation in cumulative SST anomalies throughout the entire period. The vertical yellow shading and the red line represent the corresponding years with the first abrupt SST changes (between 1996 and 2001) and the second in 2013, respectively. (D) Hovmöller diagram (daily vs. annual) of spatially averaged daily SST anomalies (seasonal cycle removed) between 1982 and 2024. The main geographical features and the isobaths (grey contour lines) of 20, 40, and 200 m are shown in panel (A).

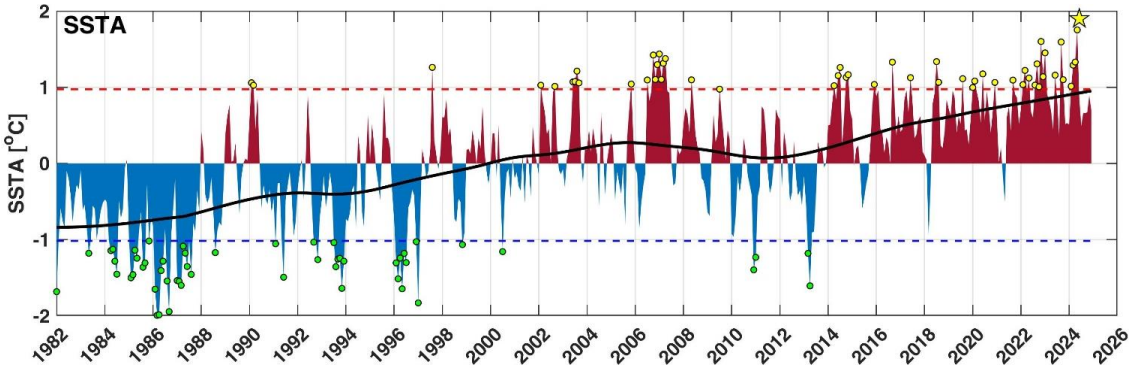

Figure 2: Temporal evolution of regionally averaged sea surface temperature anomalies (SSTA) between 1982 and 2024. The thick black line represents the SSTA trend calculated with the locally weighted scatterplot smoothing method (LOWESS). The yellow/green circles show warm/cold events where SSTA was greater/smaller than the defined 90/10 percentiles (red/blue dashed horizontal lines), which were chosen to be seasonally independent for simplicity (i.e., fixed thresholds). The yellow star refers to the highest SSTA value recorded in May 2024.

https://doi.org/10.5194/egusphere-2025-1578
Preprint. Discussion started: 16 April 2025

3.2 Pre-2013 versus post-2013 Marine Heatwaves

To investigate the regions with significant changes in mean SST, we examined the spatial distribution of mean SST differences between the post- and pre-2013 periods. The composite SST difference showed significant warming anomalies with average anomalies of 0.77°C over the entire North Sea, exhibiting an increasing zonal SST gradient from west to east (Fig. 3A). The largest anomalies were observed along the Belgian, Dutch, and Danish coasts, with an increase of up to 1.5°C in the German Bight and the Kattegat region. As highlighted in a previous study (Mohamed et al., 2023), a higher SST trend and MHWs were observed in the German Bight. These results suggest that the North Sea experienced a significant increase in mean SST after 2013, which could increase the probability of MHWs (Frölicher and Laufkötter, 2018). Therefore, we followed Frölicher et al. (2018) to investigate how the increase in mean SST could affect MHWs. Specifically, we quantified the annual mean probability ratio (PR, i.e. the fraction by which the number of MHW days changed per year) and the FAR of MHW days, as well as the relative change in the annual mean of the MHW spatial extent (i.e. the average area of a single MHW) (Fig. 3B). The regional changes in the PR and FAR of the MHW days were also calculated between the two periods (post-and pre-2013) divided by the pre-2013 period (Fig. 3C-D).

During the period before the first climate shift (i.e., from 1982 to 2001), the PR was less than one, and the FAR was almost zero (Fig. 3 B), which means that the likelihood of occurrence of the MHW days is very low compared to the entire study period. During the transition period, only 2002/2003 and 2006/2007 had a higher PR and FAR. During the post-2013 period, the PR increased by 2-5 times and the FAR also shows an increase between 25 % and 80 % (Fig. 3B). Throughout the entire study period, the most active MHW years (2006, 2007, 2014, 2020, 2022, 2023, and 2024), were those that showed an increase in FAR (more than 60 %). An increase in the spatial extent of the MHW was also observed in these years (black line in Fig. 3 B). The cumulative trends (i.e., the annual trend multiplied by the number of years out of 43) show a significant increase in PR (2.6 per 43 years) and SST (1.65°C per 43 years). The observed temporal development of the annual mean SST (green line in Fig. 3B) correlates strongly with the PR ($r = 0.80$, $p>0.05$) and the spatial extent of the MHW ($r = 0.72$, $p>0.05$). These results indicate that the change in the occurrence of MHW is mainly due to the increase in mean SST.

The regional MHW days probability ratio (i.e., the MHW probability of the post-2013 period to the pre-2013 period) had increased by 3.6 on average and ranged (from 1.6 to 9.6) (Fig. 3C). The highest PR was found over the English Channel, the Dover Strait, and the southern part of the North Sea, while the lowest values were found over the deep northern region, especially along the Norwegian coasts. This result means that the average probability of a MHW day occurring post-2013 is typically 3.6 times higher than in the period before 2013 (Fig. 3C). This sharp increase in PR and warming conditions was also associated with an increase in the attributable risk fraction, which averaged 69% and ranged from 40% to 90% (Fig. 3 D). Similarly, the FAR for the frequency and duration of MHW was calculated and showed a 64% increase in the frequency of MHW events and a 24% increase in duration in the most recent post-2013 period compared to the earlier pre-2013 period.

https://doi.org/10.5194/egusphere-2025-1578
Preprint. Discussion started: 16 April 2025

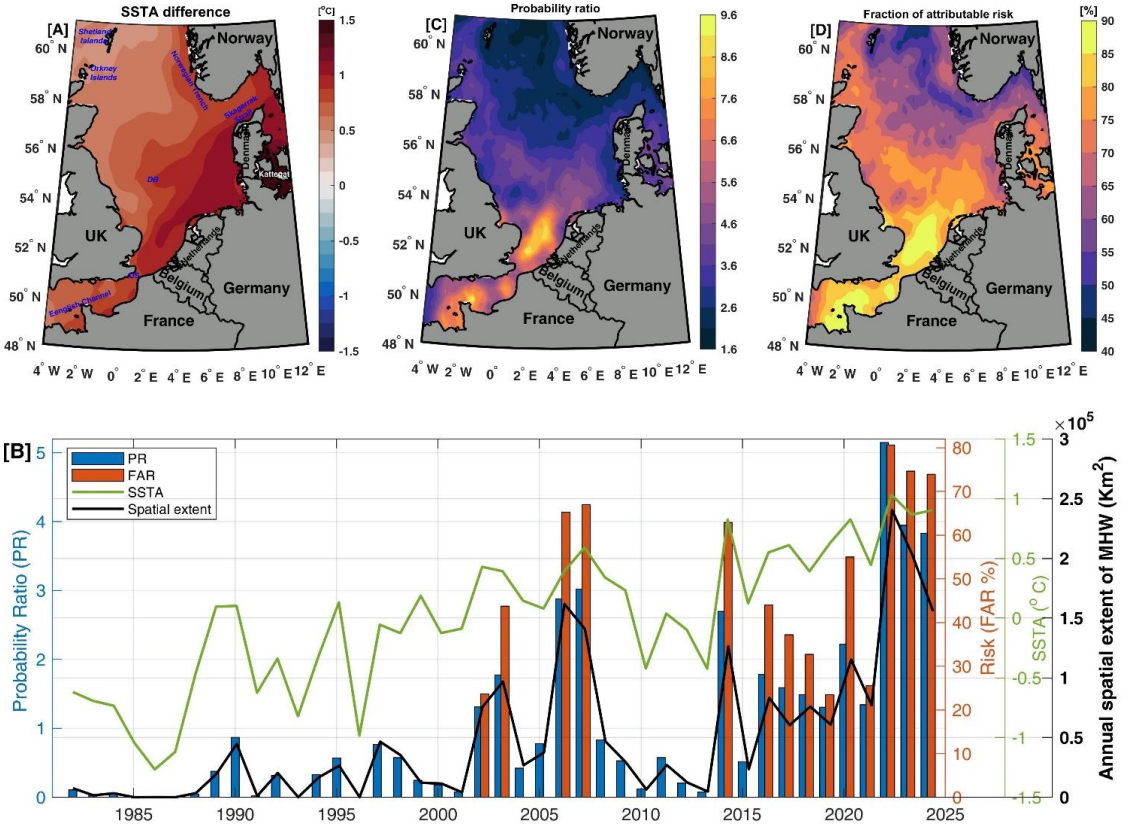

Figure 3: (A) Composite differences in annual mean sea surface temperature between 2013–2024 and 1982–2012. (B) Annual mean values of the probability ratio (PR, blue bars), the fraction of attributable risk (FAR) of MHW days, and the spatial extent of MHW (black line) throughout the entire study period. (C and D) The regional changes in the PR and FAR of MHW days in the post-2013 period compared to the pre-2013 period. Based on the standard two-sample Student's t-test, the composite mean difference is significant ($p < 0.05$) over the entire North Sea at a 95% confidence interval.

To explore how an increase in mean SST might affect the occurrence of MHW on a daily time scale, we analyzed the probability distribution function (PDF) of the daily area-averaged SSTA and the frequency of MHW occurrences in the North Sea, as shown in Figure 4. The PDF is estimated based on the Generalized Extreme Value (GEV) distribution (Li et al., 2023). Generally, the increase in internal variability of SST leads to a broadening of the PDF of temperature, making the occurrence of MHW more likely. In addition, changes in mean SST values due to the SST warming shift the center of the PDF to the higher values, which also leads to an increased occurrence of MHW (Xu et al., 2022). To verify this in our study region, we compared the change in the PDF of daily SSTA between the pre-and post-2013 periods (i.e., the last climate shift), based on the original (Fig. 4A) and detrended SSTA time series (Fig. 4B). The PDF of the original SSTA exhibits a significant peak shift in the mean SST value between the two different periods (Fig. 4A). For the post-2013 period, the peak density of the GEV-fit PDF reaches 63% at an SSTA of 0.57°C, compared to 52% at an SSTA of -0.22°C in the pre- 2013 period, with a statistically significant difference of 0.79 °C between the two periods. During the post-2013 period, there has been a clear shift towards a warmer state, indicated by the substantial increase in SSTA at the right-hand tail of the PDF, leading to an excessive trend in MHW, as shown by the area to the right of the green line marking the 90th

https://doi.org/10.5194/egusphere-2025-1578
Preprint. Discussion started: 16 April 2025

threshold (Fig. 4A). Meanwhile, the SSTA variance changes slightly (from 0.56 °C to 0.39 °C). The curve shape of the post-2013 period is notably skewed (with a skewness value of –0.65), compared to a value of 0.02 in the pre-2013 period (Fig. 4A). Consequently, the occurrence of MHWs on the skewed side would be more frequent and intense than MCSs on the non-skewed side.

To further investigate the MHW occurrences between the two periods, we calculated the frequency of MHW occurrences for each month based on the original (Fig. 4C) and detrended SST data (Fig. 4D). The frequency of MHW occurrence is higher in all months post-2013 than pre-2013, except for February and March, which show slightly higher values in the pre-2013 period (Fig. 4C). The monthly averages of the mean MHW intensity for the two periods (pre- and post-2013) show a clear annual cycle (green and black lines in Fig. 4C), with maximum values of 2°C in summer and minimum values of 1 °C in winter. The mean MHW intensity in the post-2013 period showed a seasonal shift compared to the pre-2013 period, with a more intense (warmer) and longer summer season. These results suggest that severe MHWs have occurred more frequently over the North Sea since 2013, particularly with a marked increase in MHW during the summer and fall seasons. After using the detrended SSTA for the PDF calculations (Fig. 4B), we found that the mean SST for the post-2013 period was not statistically different from that for the pre-2013 period, while the variance decreased slightly. In addition, the occurrence of MHW decreased in the post-2013 period compared to the pre-2013 period (Fig. 4D). These results indicate that the increase in mean SST (or long-term warming), rather than SST variability, plays a dominant role in the development of the long-term trend in MHW over the North Sea.

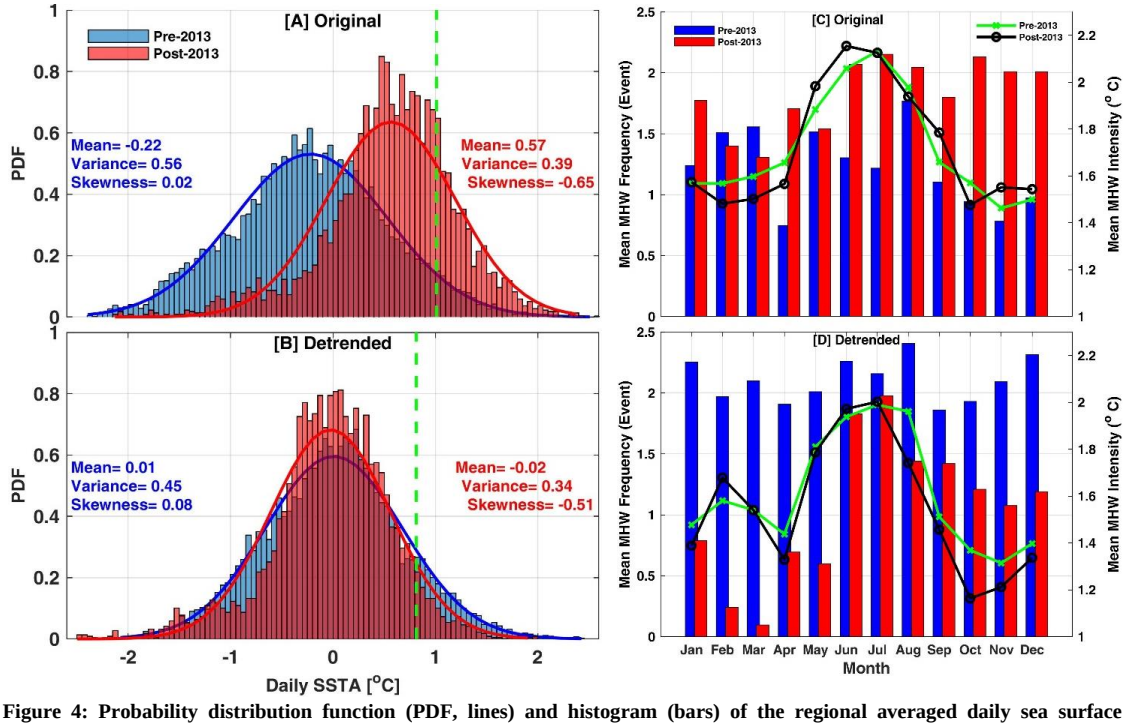

Figure 4: Probability distribution function (PDF, lines) and histogram (bars) of the regional averaged daily sea surface temperature anomaly (SSTA) during the pre-2013 period (1982–2012, blue) and the post-2013 period (2013–2024, red), based on the original (A) and detrended SST data (B). The vertical green dashed line refers to the 90th threshold temperature of the MHW. Monthly mean MHW frequency (bars) and MHW intensity (lines) from the original (C) and detrended SST data (D) for the pre-2013 period (blue bars and green lines) and post-2013 (red bars and black lines).

https://doi.org/10.5194/egusphere-2025-1578
Preprint. Discussion started: 16 April 2025

3.3 Effects of the SST long-term trend and variability on MHWs

In this section, we analyze how the interannual variability of SST and long-term warming affect the long-term MHW trend in the North Sea over the entire period (1982 to 2024). The sensitivity of MHW in response to an increase in mean SST varies regionally (Lee et al., 2023). To date, no study has evaluated the relative role of the long-term trend and internal variability on the MHW in the North Sea. Therefore, we first investigate the linear trend maps for the annual mean of SSTA and the variance (Fig. 5). The SSTA trend is significant throughout the region, with an increasing zonal gradient from west to east (Fig. 5A). The strongest SST trends are observed over the Kattegat and the German Bight. The SSTA variance shows an insignificant trend across the North Sea, except for the German Bight and the Norwegian Trench, where significant negative variance trends are observed in these regions (Fig. 5B). Then, to investigate the spatiotemporal patterns of MHW and their linear trends in the North Sea, we perform an empirical orthogonal analysis (EOF) and the corresponding principal components (PC) for the MHW. Since the cumulative intensity can simultaneously reflect the frequency, duration, and mean intensity of the MHW (Jin and Zhang, 2024), we applied the EOF analysis to the annual cumulative intensity of the MHW (Fig. 6).

The first two EOF modes of cumulative MHW intensity account for 78.9% of the total variance. The spatial pattern of the leading first EOF mode (EOF1, explains 69.5 %) shows high positive values over the entire study area (Fig. 6A), indicating an in-phase increase in MHW over the entire North Sea. The highest variability in cumulative MHW intensity is found over the shallow central region of the study area and the Dogger Bank (see the location in Fig. 1A). These regions are influenced by both warm Atlantic Water from the north/south of the North Sea opening and cold water from the Baltic Sea. The corresponding principal component of EOF1 (PC1) shows a significant (at 95% using the MMK test) increasing linear trend, especially after 2001 (i.e. the first climate shift) and more pronounced after 2013 (i.e. the second climate shift), indicating that MHW in the North Sea was more intense and prolonged after these climate shifts (Fig. 6C). Moreover, PC1 shows significant interannual variability, with the highest substantial increase of the cumulative MHW intensity occurring in 2003, 2006/2007, 2014, and the last three years (2022–2024), which coincide with the positive phases of the AMO index (Fig. 6C). The strong 2003, 2014, and 2023 MHWs in the southern North Sea have been reported by (Berthou et al., 2024; Mohamed et al., 2023).

The second EOF mode (EOF2, explains 9.4 %) is a regional variability mode and shows a dipolar oscillation with opposite fluctuations between the northeastern part of the study area and the southern and northwestern parts (Fig. 6B). The maximum variability is found over the regions influenced by the inflow of fresh and cold water from the Baltic Sea via the Skagerrak Strait. In contrast, the opposite maximum variability is observed over the regions influenced by the inflow of warm and salty Atlantic water. The PC2 does not show long-term warming, it is therefore mainly projected onto the interannual and decadal variability (Fig. 6D). From the PC2 time series, an increase in the amplitude of oscillations is evident, especially when comparing the period before and after 2001, which corroborates a negative trend in variability intensity. Therefore, PC1 is associated with the long-term trend, and PC2 with the variability, which may also contain variability and a trend. We also examined the relationship between the PCs and the normalized indices of AMO and EAP (bars and green line in Fig. 6C). Both AMO and EAP showed a significant correlation of 0.66 and 0.50, respectively, with the first PC1. During the post-2013 period, the most active MHW years coincide with the strongest positive phases of both AMO and EAP indices. During the period before the first climate shift (1982–2001), the negative values of PC1 are

https://doi.org/10.5194/egusphere-2025-1578
Preprint. Discussion started: 16 April 2025

associated with negative phases of AMO and/or EAP. These results are consistent with those of Mohamed et al. (2023), who found a strong correlation between SST and both AMO and EAP on the interannual time scale in the southern North Sea. They also found that 45 % and 35 % of the total observed MHWs were associated with the positive phases of the EAP and AMO indices, respectively.

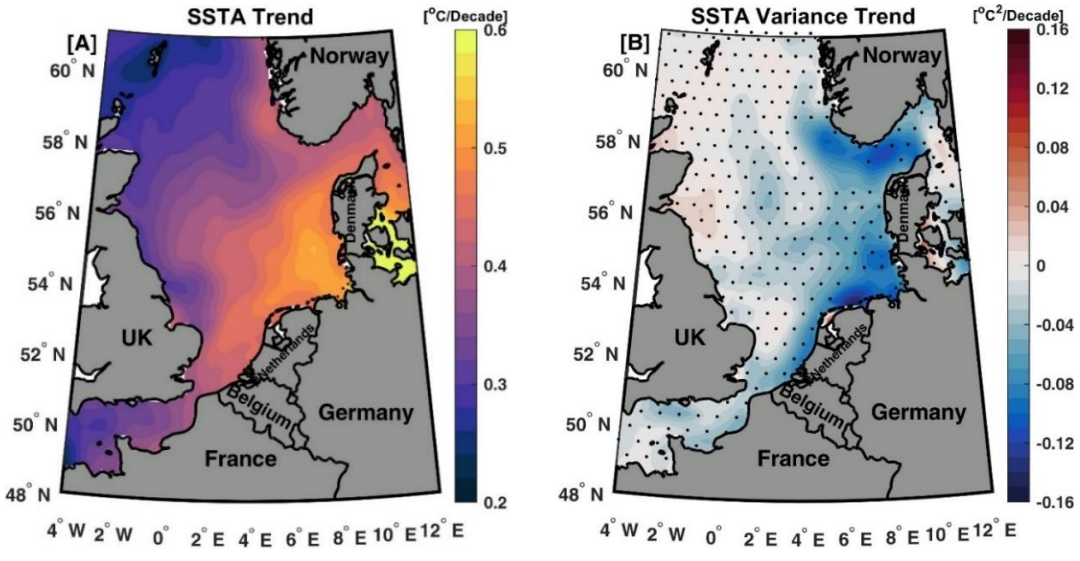

Figure 5: Linear trend maps for the annual mean of (A) the sea surface temperature anomaly (SSTA) and (B) the variance of the SSTA during the period 1982–2024. The dotted areas indicate that the trend is insignificant at a 95% significance level.

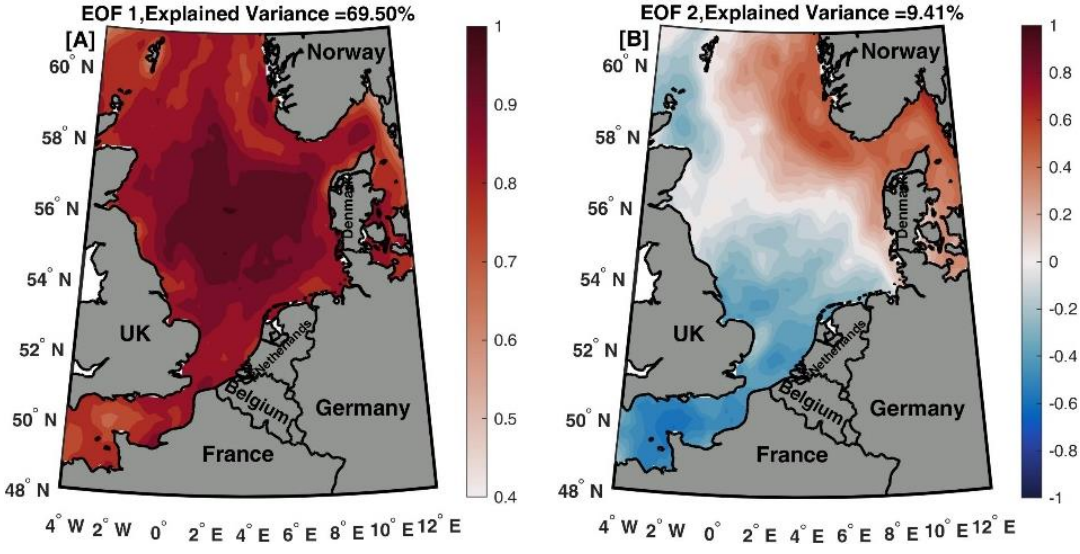

https://doi.org/10.5194/egusphere-2025-1578
Preprint. Discussion started: 16 April 2025

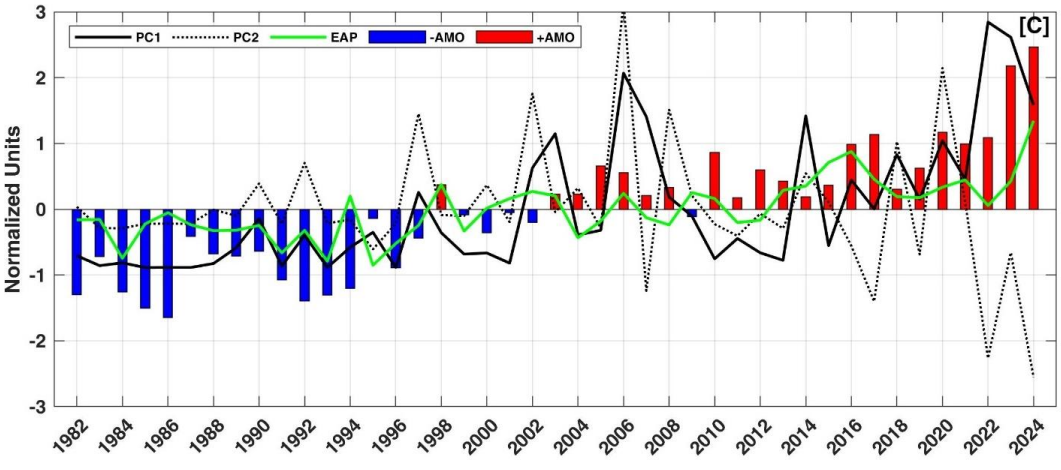

Figure 6: The two leading EOF modes of cumulative MHW intensity in the North Sea (A and B), and their corresponding normalized principal components (C) over the period 1982–2024. In panel (C), the bars represent the normalized AMO index, and the green line is the EAP index.

Quantifying the role of climate change on increasing MHW characteristics depends on identifying the long-term externally forced SST warming trend separately from changes in internal variability (Oliver, 2019; Xu et al., 2022). Therefore, we evaluate the influence of the long-term SST warming on the MHW by removing the linear trend from the original SST at each grid point to obtain a detrended SST. We then used the detrended daily SST to re-determine the MHW characteristics based on the same climatological baseline (1982–2024). Thus, the MHW resulting from the detrended SST is only related to the internal variability and not to the long-term trend of the SST.

The relative contributions of the long-term trend and the internal variability of the SST to the overall increase of the MHW characteristics (frequency and cumulative intensity) from 1982 to 2024 are estimated and compared in Figure 7. The MHW frequency calculated from the original SST (red line in Fig. 7A) shows a significant increase of 1.04 ± 0.29 events/decade. On average, 80 MHW events were detected over the entire study period; 55% of these events (44 events) were detected in the post-2013 period, with 26 events occurring in the five active MHW years (2014, 2020, 2022, 2023, and 2024). In contrast, the MHW frequency obtained from the detrended SST (black line in Fig. 6A) shows an insignificant negative trend with a decrease in the total number of MHW events from 44 to 15 in the post-2013 period. The difference between these two values (the former minus the latter) is attributed to the long-term SST trend, which shows a similar/slightly higher trend than the original SST (green line in Fig. 7A).

The time series of the cumulative MHW intensity from the original SST, the detrended SST, and their difference in the period from 1982 to 2024 are shown in Figure 7B. The trends of the cumulative MHW intensity of the original SST show a significant increase of 4.23 ± 0.1.98 (°C. days)/decade, with the highest cumulative intensity in 2022 and 2023. The difference between the result from the original minus the detrended data shows a higher significant trend of 5.24 ± 1.55 (°C. days)/decade (Fig. 7B). Compared to the original time series (red lines in Fig. 7), the MHW frequency and cumulative intensity resulting from the detrended SST data (black lines in Fig. 7) show insignificant decreasing trends. These results indicate that the long-term SST trend is the main driver for the observed long-term trend of MHW in the North Sea region, which confirms the crucial role of the mean SST changes on the MHW in this region.

https://doi.org/10.5194/egusphere-2025-1578
Preprint. Discussion started: 16 April 2025

The spatial variability of the annual average of MHW days for the active MHW years (2014, 2020, 2022, 2023, and 2024) is shown in Figure 8. The occurrence of MHW based on the original SST shows that there were at least five MHW events per year in these active MHW years (red line in Fig. 7A), which is consistent with the same years showing a high SSTA (green line in Fig. 3B). The annual average of MHW days determined using the original SST (upper panels in Fig. 8) show that between 17 % (61 days in 2020) and 34 % (123 days in 2022) of the days of the year experience MHW, while this value is reduced with the detrended data (lower panels in Fig. 8) and lies between 3 % (11 days in 2020 and 2024) and 8 % (31 days in 2014). The detrended method generally shows fewer MHW days than those determined using the original SST data. The regions where the SST warming trend is stronger (e.g., the German Bight) show, on average, more MHW days from the original SST data than those obtained from the detrended approach. Both approaches (the original and the detrended) show high year-to-year variability in MHW days, suggesting that SST variability and thus MHW in the North Sea are largely influenced by atmospheric rather than oceanic forcing, which is consistent with Tinker and Howes (2020).

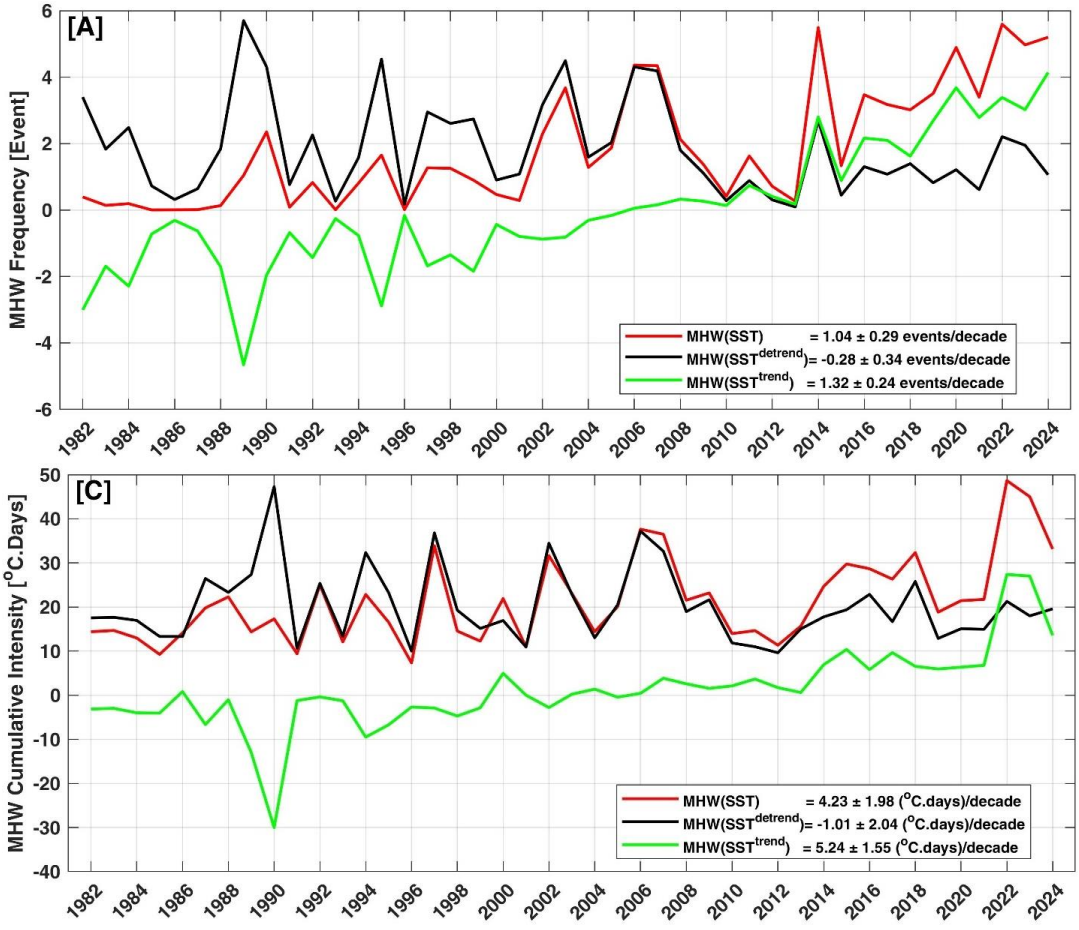

Figure 7: Temporal evolution of the annual (A) MHW frequency and (B) cumulative mean intensity from 1982 to 2024. The red and black lines in (A and B) represent the time series calculated from the original and detrended SST, respectively. The green lines are the differences between the original and detrended results.

https://doi.org/10.5194/egusphere-2025-1578
Preprint. Discussion started: 16 April 2025

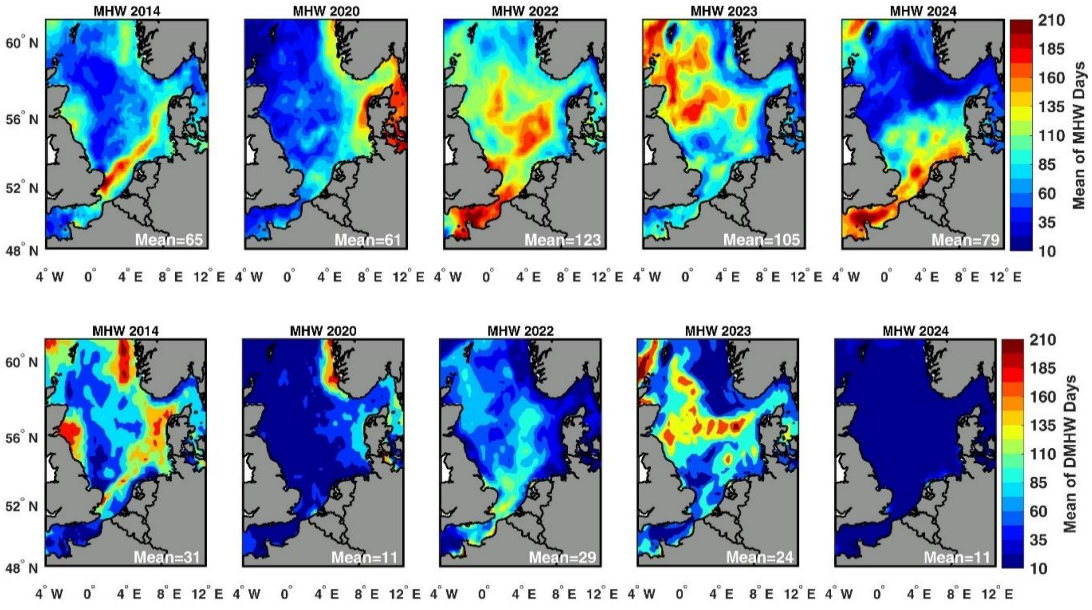

Figure 8: Spatial maps of the annual average of MHW days based on the original SST (upper panels) and detrended SST (lower panels) for the active MHW years 2014, 2020, 2022, 2023, and 2024.

To further investigate the drivers of MHW trends at the regional scale, we estimate the trend attribution ratio (TAR) for MHW frequency and MHW cumulative intensity (Fig. 9). The TAR metric assigns the proportion of the MHW trend over 43 years (1982–2024) that is attributable to long-term changes in mean SST and residual internal variability (Marin et al., 2021). The positive TAR values for both MHW frequency and MHW cumulative intensity over the entire North Sea (Fig. 9) indicate that the trends in MHW frequency and MHW cumulative intensity are largely explained by the long-term changes in mean SST. The TAR values ranged from 0.4 to 1 for MHW frequency (Fig. 9A), and from 0.3 to 1 for MHW cumulative intensity (Fig. 9B), with an average of 0.80 and 0.78, respectively. The lowest TAR values for the MHW cumulative intensity coincide with the same regions (i.e., German Bight, Norwegian Trench) that showed significant negative trends in SST variance (Fig. 5B). The possible explanation is that the changes in internal variability contribute to a decrease in the MHW trend in these regions. These results imply that, on average, 80% (78%) of the observed trends in MHW frequency (cumulative intensity) are due to the long-term SST trend, while the remainder is attributed to internal variability.

https://doi.org/10.5194/egusphere-2025-1578
Preprint. Discussion started: 16 April 2025

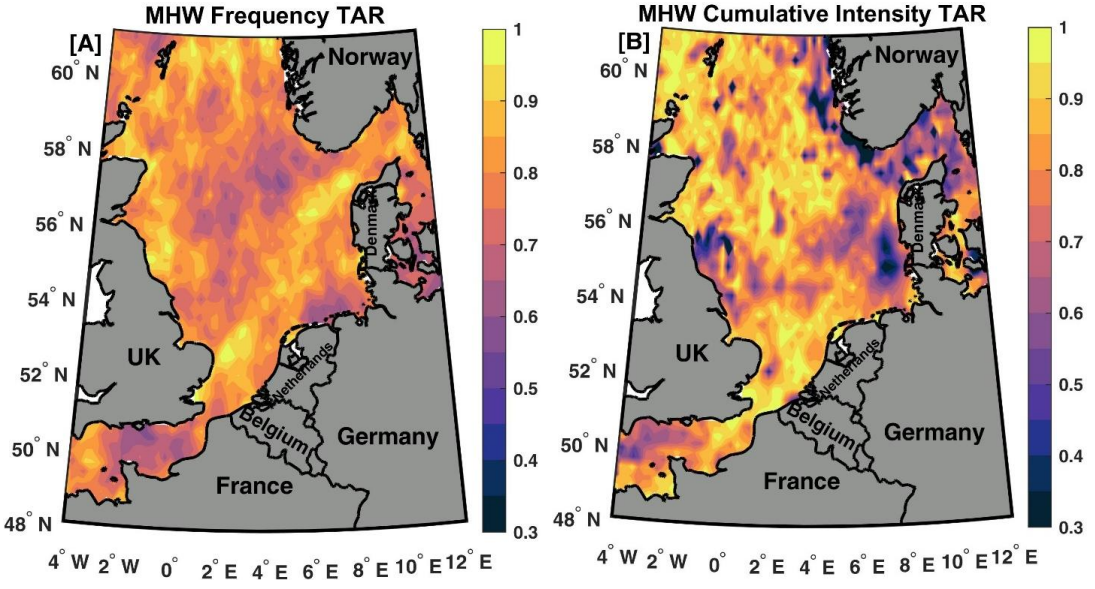

Figure 9: Trend Attributional Ratio (TAR) maps of the trends in (A) MHW frequency and (B) MHW cumulative intensity over the period (1982–2024). The positive TAR values over the entire area show the stronger influence of the mean SST changes on the observed MHW trends in the North Sea.

395

3.4 Spring 2024 New Record SST and MHW

The highest monthly SSTA record in the North Sea was reached in May 2024 (yellow star in Fig. 2), this record was manifested by the extreme MHW from May 10 to July 5, 2024 (yellow shaded area in Fig. 10A). In this section, we focus on the causes of this extreme MHW event. Daily SSTA remained exceptionally high, with May 2024 being the second
400 warmest period on record for this time of year after July 2014 (Fig. 10B). The third SST record was observed in June and September 2023, which were associated with an exceptional MHW in northwestern Europe (Berthou et al., 2024). The most active MHW years during the entire study period were observed post-2013 climate shift, which demonstrated a strong positive SSTA (Fig. 3B) and at least five MHW events per year (Fig. 7). According to the MHW severity classification (Hobday et al., 2018), the intensity of all these events can be categorized as moderate MHW, where the SSTA exceeds the
405 90th percentile threshold anomalies (Fig. 10B).

The highest daily SSTA in 2024 was recorded in the first half of this year, mainly from mid-February to early June (red bars at the bottom of Fig. 10A). During this period, five MHW events were detected where the daily SST (red line in Fig. 10B) exceeded the 90th percentile threshold (dashed black line in Fig.10B). The duration of these events ranged from 5 to 27 days. The longest (27 days) and most intense (2.2°C) MHW event occurred between May 10 and July 5, 2024 (spring
410 2024 MHW, hereafter). This event covered most of the North Sea (96% of the total area), with the SSTA ranging from 0.55 to 4°C (Fig. 11A). The spatial pattern of the SSTA shows a zonal gradient with the lowest value in the west (around the coasts of the United Kingdom and the English Channel) and the highest value in the east (around the coasts of Norway and Denmark and in the German Bight). Atmospheric conditions during this event showed warm surface atmospheric temperature anomalies (SATA) over the entire region (Fig. 11B), with the same pattern as the SSTA over the ocean. The

https://doi.org/10.5194/egusphere-2025-1578
Preprint. Discussion started: 16 April 2025

415 highest SATA values were found over the eastern coasts, which coincides with the same region experiencing the highest MHW intensity. Over the land, the highest SATA was found in Norway and the lowest in France. This suggests that atmospheric overheating and thus weather conditions could best explain this MHW event.

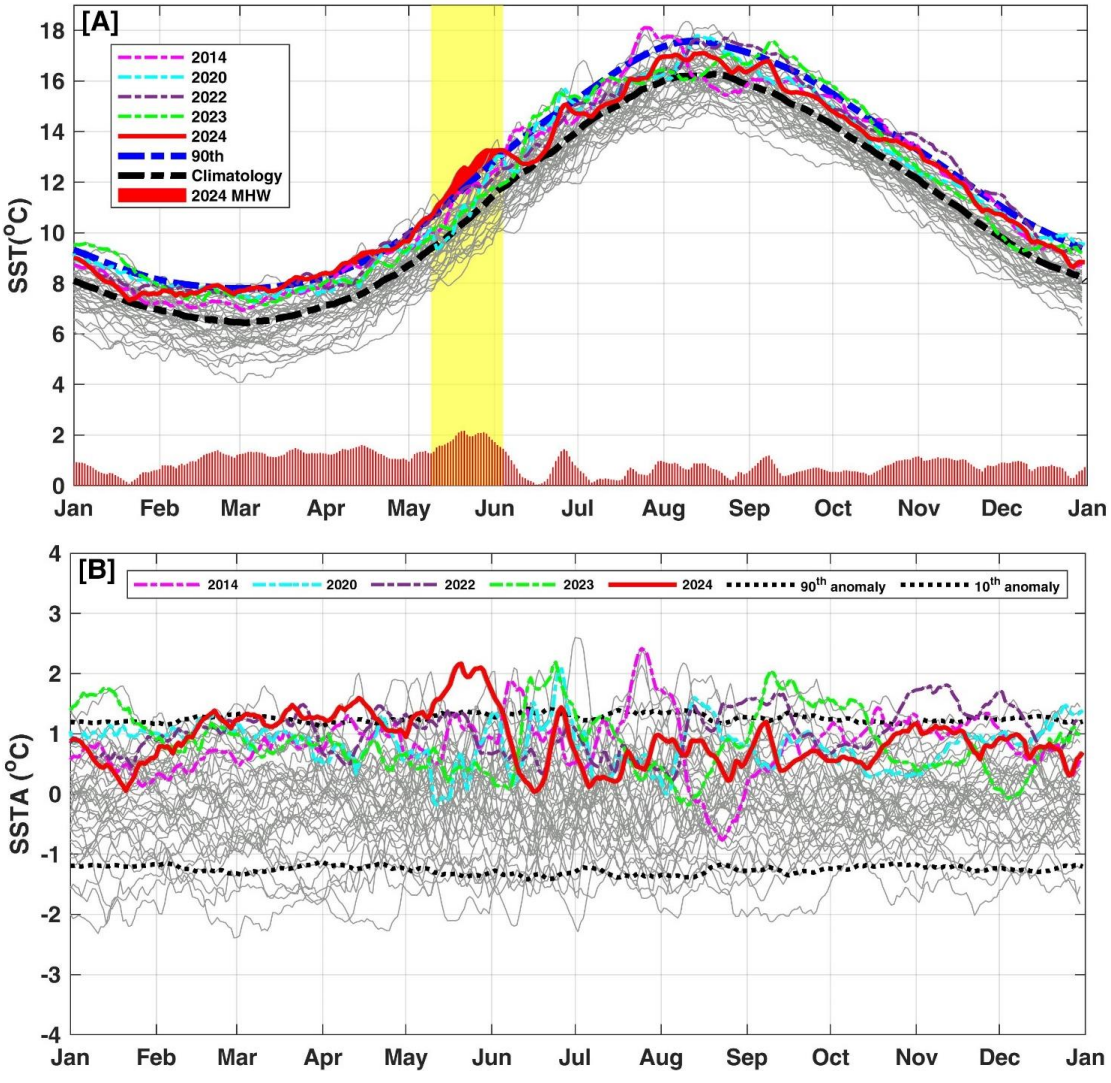

420 **Figure 10: Regionally daily averaged (A) sea surface temperature (SST) and (B) sea surface temperature anomaly (SSTA) from 1982 to 2024, represented by gray lines, except for the active MHW years (2014, 2020, 2022, 2023, and 2024). In (A), the dashed black/blue lines represent the climatology/90th percentile of daily SST. The daily SSTA during 2024 is shown in red bars at the bottom of panel (A), and the vertical yellow shading represents the MHW occurring from May 10 to July 5, 2024. In (B), the 90th/ 10th percentile anomalies are represented by black dotted lines. Note that, all the anomalies were calculated by subtracting the**
425 **climatological daily SST (computed over 1982–2024).**

https://doi.org/10.5194/egusphere-2025-1578
Preprint. Discussion started: 16 April 2025

The question, therefore, arises as to what the main causes of this atmospheric overheating and the MHW event in spring 2024 are. We address this question by examining the decomposition of all atmospheric factors, including cloud cover, heat budget components, wind components, atmospheric pressure, and geopotential height. During this event, the total cloud cover anomalies over most of the North Sea are always negative, with the highest negative anomalies (up to 20%) occurring in the core region with the highest intensity of the MHW (Fig. 11C). As a result of the reduction in total cloud cover, the shortwave radiation has increased over most of the North Sea (Fig. 11D), except in the region around the Strait of Dover where negative shortwave radiation anomalies are accompanied by positive cloud cover anomaly. The contrasting pattern of cloud cover and shortwave radiation demonstrated their relatedness. The average increase in shortwave surface radiation during this MHW event was 6 W/m^2 compared to the daily climatological mean at this time of year (calculated over 1982–2024). These abnormal climate conditions could be responsible for the high atmospheric and oceanic temperatures that eventually triggered the spring MHW.

The wind during this MHW event is weaker than the daily climatological mean at this time of year (calculated over 1982–2024), with negative wind anomalies across the region (shading in Fig. 11E). This weaker wind speed could lead to less mixing of the water column and thus to strong stratification and overheating of the surface water temperature. In addition, the geopotential height anomalies at 500 hPa during this MHW event show a strong anomalous anticyclonic circulation centered over the northern Baltic Sea (Fig. 11F), with the area under the high-pressure anomalies (up to +3.5 hPa) dominated by subsidence. The edge of this circulation extended into the northern part of the North Sea. This anticyclonic circulation favors the reduction of total cloud cover, leading to increased solar radiation and further warming of the upper ocean through air-sea interactions (i.e., conditions that are favorable for the occurrence of the MHW). In addition, cyclonic atmospheric patterns with lower air pressure anomalies (less than -1.5 hPa) are observed over France and Belgium. As a result of these two atmospheric systems, the wind anomalies over the North Sea were dominated by easterly and south-easterly winds (arrows in Fig. 10E), which led to the transport of warm continental air masses over the sea.

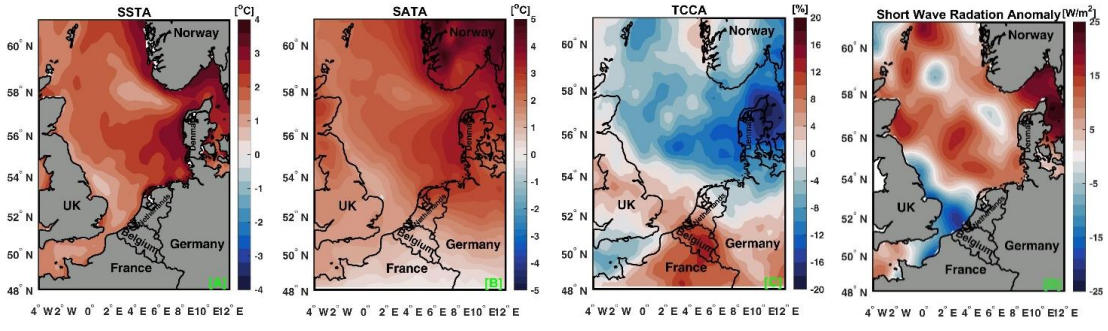

https://doi.org/10.5194/egusphere-2025-1578
Preprint. Discussion started: 16 April 2025

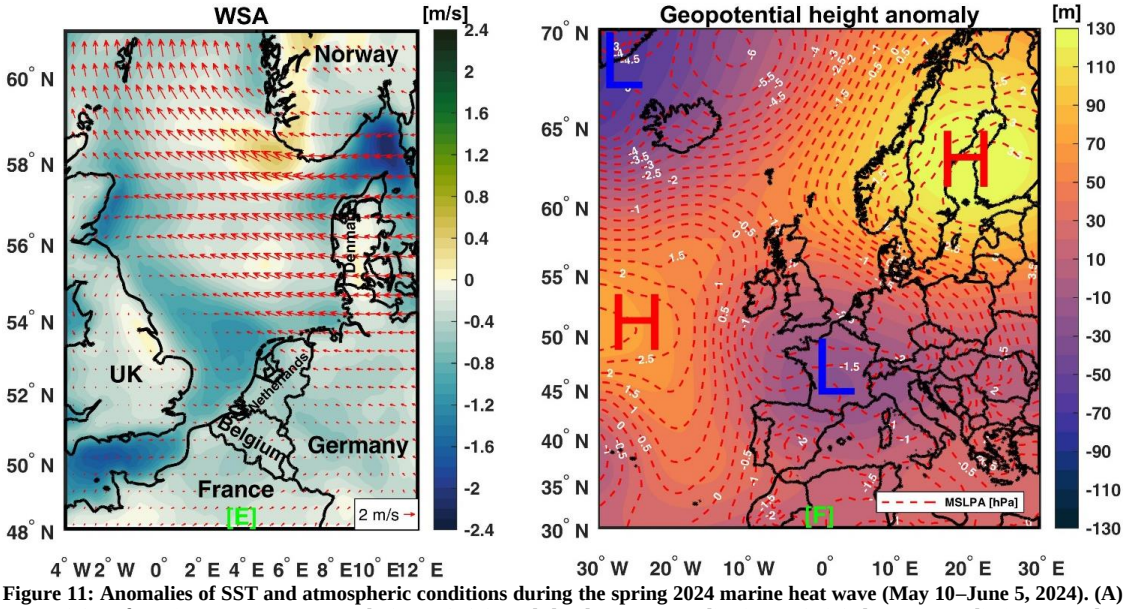

Figure 11: Anomalies of SST and atmospheric conditions during the spring 2024 marine heat wave (May 10–June 5, 2024). (A) SSTA, (B) surface air temperature anomaly (SATA), (C) total cloud cover anomalies (TCCA), (D) shortwave radiation anomalies (SRA), (E) wind speed anomalies (WSA, shading is the magnitude and vectors are wind direction), (F) geopotential height anomalies (GPHA) at 500 hPa, the dashed contour lines represent the anomalies of the mean sea level pressure (hPa). All anomalies were calculated by subtracting the daily climatological SST (calculated over 1982–2024).

3.5 Biological Impact of MHW and MCS

To assess the biological impact and responses of phytoplankton biomass to MHW and MCS in the North Sea, we analyzed the fluctuations of chlorophyll-a (CHL), which is considered a proxy for phytoplankton biomass and primary productivity (Alvera-Azcárate et al., 2021). First, we investigate the seasonal CHL variation and trend, and the spatial correlation between the de-seasonalized monthly CHL and SST (Fig. 12). Then, we redetermined MHWs and MCSs based on the monthly approach and the climatological baseline of the period overlapping with CHL (1998–2024) to assess their impact on CHL (Fig. 13). The climatological daily CHL seasonal cycle (Fig. 12A) shows that the highest variability of CHL occurs in April and May, which are characterized by the spring phytoplankton bloom (Amorim et al., 2024), with an average monthly CHL concentration of 2.2, 3.1, 3.0, and 2.2 mg/m^3 for March, April, May, and June, respectively. The monthly trend analysis of the CHL shows a smaller but still significant positive trend in February and March. In contrast, a significant negative trend was observed in May, while no significant trends were observed in the other months, as the uncertainties were higher than the trend values (boxplots in Fig. 12A). A possible explanation for the contrasting CHL trends (i.e., positive in February and March and negative in May) is that the onset of the spring bloom in the North Sea has been observed to start earlier each year, especially after the 2009 period (Alvera-Azcárate et al., 2021). The average CHL concentration increased from February to mid-April, while it decreased from mid-April to mid-June after 2009 (red line in Fig. 12A) compared to the period before 2009 (blue line in Fig. 12A). The strongest CHL decline after 2009 is recorded in the first half of May, which is seen as part of the observed negative CHL trend in the North Sea. This result confirms the change in the onset of the occurrence of the spring bloom in the North Sea, which could be due to the seasonal SST shift and the occurrence of MHW (Fig. 4C). As in the latest period, the CHL concentration increased/decreased from February to April/

https://doi.org/10.5194/egusphere-2025-1578
Preprint. Discussion started: 16 April 2025

(from May to June) compared to the earlier period (Fig. 12A), which coincides with the decrease/increase in the intensity of MHW in the same months (Fig. 4C).

A high spatial variability of the de-seasonalized monthly CHL trends can be observed in the North Sea (Fig. 12B). The strongest negative trends (between -0.4 and -0.8 mg/m^3/decade) are found in the north-eastern corner of the study area (i.e., around the coastal regions of Norway and Denmark), along the French coast, in the Wadden Sea and the deep part west of the Dogger Bank (Fig. 12 B). In contrast, the most significant positive CHL trends (between +0.4 and +0.8 mg/m^3/decade) are recorded along the south-east coast of the UK and in the south-central part of the study area, which is influenced by nutrient-rich freshwater inflows from the rivers Thames, Bure, Waveney, Wang, Blyth, and Deben along the southernmost coast of the UK. Positive trends are also observed along the Belgian coast and in the eastern German Bight, which is influenced by nutrient-rich freshwater inflows from rivers, such as the Scheldt and Elbe.

The correlations between the de-seasonalized monthly data of both CHL and SST showed a direct (inverse) relationship over the southern (northern) part of the North Sea. Significant ($p<0.05$) positive correlations are observed along the Belgian and Dutch coasts and in the Kattegat and German Bight, as well as in some areas around the southern and eastern coasts of the UK (i.e., in the main regions with positive CHL trends). Significant ($p<0.05$) negative correlations are found on the Norwegian coasts and in the eastern region of Denmark, while most other areas show an insignificant relationship ($p>0.05$).

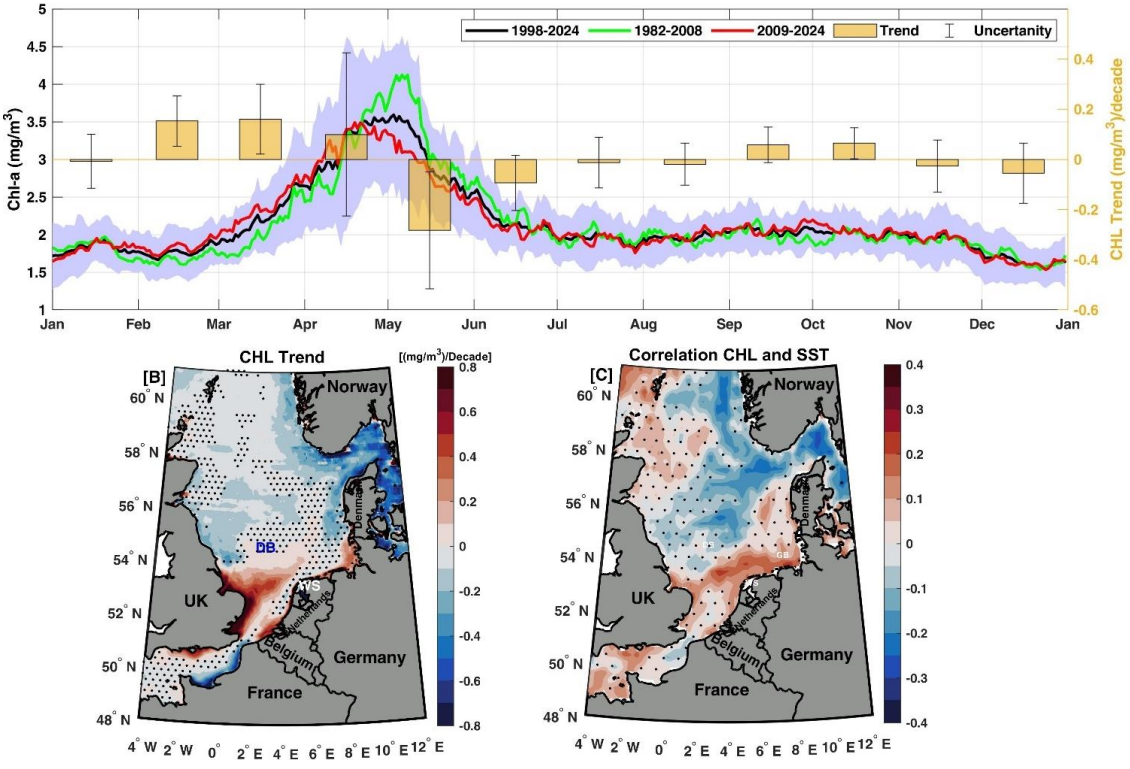

Figure 12: (A) The average CHL daily seasonal cycle over the entire North Sea for the entire period (1998–2024, black line), before and after 2009, green and red lines, respectively. The shaded area represents the ± standard deviation. The box plots show the monthly trend of CHL with the associated uncertainty. (B) Trend map of CHL (mg/m3/decade) and (C) correlation between CHL and SST during the whole period (1998–2024). The seasonal cycles were removed from both time series before estimating the trend and correlation.

https://doi.org/10.5194/egusphere-2025-1578
Preprint. Discussion started: 16 April 2025

To better assess the impacts of MHW events on CHL concentrations in the North Sea, we first identify the MHWs based on the new baseline of the overlap period with the CHL data (1998–2024). The results reveal that there are 32 MHW events and 23 MCS events (Fig. 13A). Then, we analyze the coexistence of these events (i.e., MHWs and MCSs) with the CHL anomaly (CHLA) calculated in terms of their general distribution as described in (Chauhan et al., 2023). The average CHLA during all MHW and MCS events is shown in Figures 13B and C. During the MHW events, negative CHLA values are observed in the central and northeastern parts of the North Sea. In contrast, positive CHLA values are predominantly found in the southern North Sea (especially along the coastal areas of Belgium, the Netherlands, the German Bight, and the south-eastern coast of the United Kingdom, as well as in the western part of the English Channel) and around the Shetland Islands in the northwestern part of the study region (Fig. 13B). The opposite pattern of CHLA is observed during the MCS events (Fig. 13C). The composite CHLA difference (during MHW minus MCS) shows insignificant changes over most of the North Sea (Fig. 13D), except along the Norwegian Trench, the Skagerrak Strait and the central regions, where a significantly negative CHLA difference is observed (i.e., in the same areas that correlate negatively with the SSTA, Fig. 12C). In contrast, a significantly positive CHLA difference is observed along the coastal regions of Belgium, the Netherlands, the German Bight, and the south-eastern coast of the United Kingdom, as well as around the Shetland Islands (Fig. 13D). The complex interaction of CHL with SST and MHW confirms that there are other factors influencing CHL concentrations in the North Sea in addition to the sea surface warming, such as changes in nutrient inputs from the rivers (Desmit et al., 2020; Jacobs et al., 2024).

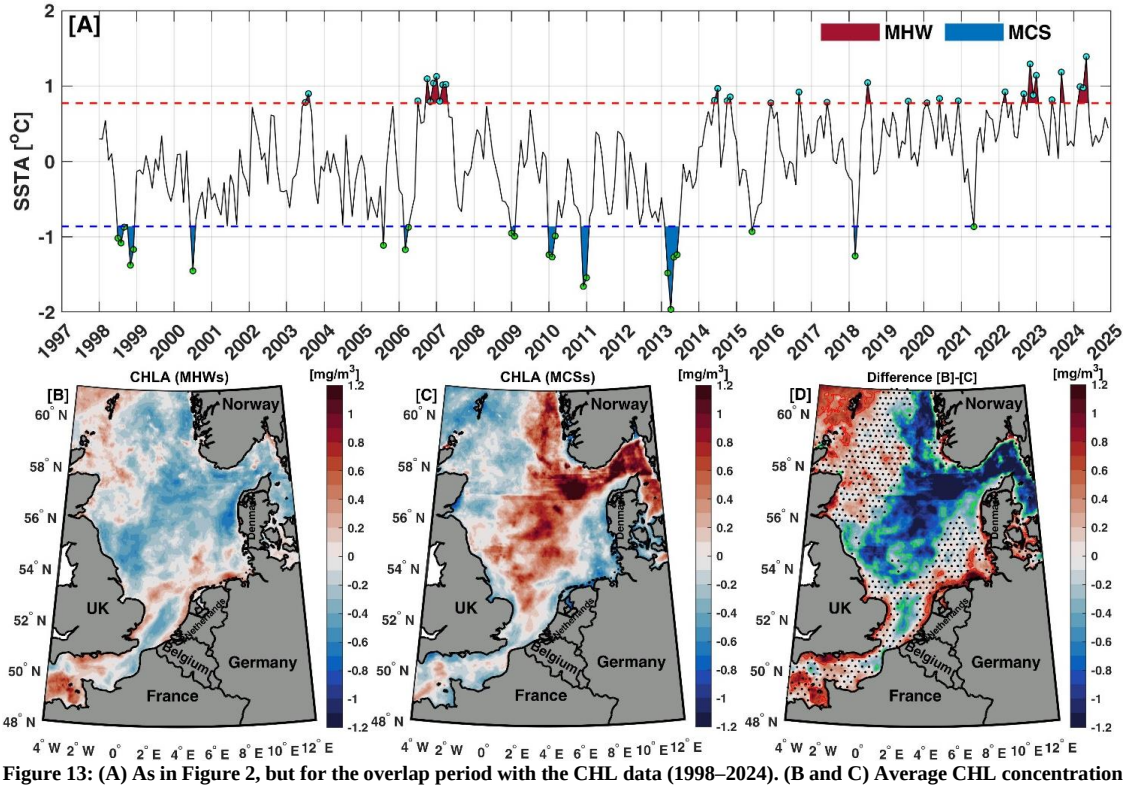

Figure 13: (A) As in Figure 2, but for the overlap period with the CHL data (1998–2024). (B and C) Average CHL concentration anomalies (CHLA) during all MHW and MCS events. (D) Composite differences in CHLA between MHW and MCS events. In (D), the dotted areas indicate that the change is not significantly different from zero based on the standard two-sample Student t-test at the 95% confidence interval (p > 0.05). The regions bounded by the green/white contour line refer to the region that shows a significant negative/positive difference, respectively.

https://doi.org/10.5194/egusphere-2025-1578
Preprint. Discussion started: 16 April 2025

4. Conclusions

In this article, we considered different MHW approaches, including fixed, seasonally varying thresholds and detrended methods, to investigate the relative contribution of the long-term warming trend and internal variability to the observed trends in MHW characteristics in the North Sea over more than four decades (1982–2024). In addition, we investigated the biological impacts and responses of phytoplankton biomass to MHW during the overlap period with the chlorophyll data (1998–2024).

The SST analysis showed a significant warming trend of 0.38°C/decade between 1982 and 2024, with the strongest increase in the Kattegat and the German Bight. This study revealed two abrupt increases in mean SST in the late 1990s and 2013. These regime shifts were attributed to the reversal of the AMO and EAP from a negative to a positive phase. Here, we focused on the recent climate shift in 2013 and investigated how the increase in average SST affects the daily SST probability density function and the occurrence of MHWs in the North Sea. Our results indicate warmer conditions in the post-2013 period compared to the pre-2013 period, with a zonal SST gradient (i.e., from west to east) and a significant increase of 0.77°C in mean SST over the North Sea.

The North Sea is most likely a high-risk region for the impacts of MHW, as we observed a rapid increase in MHW frequency (1.04 events/decade) and cumulative intensity (4.23 ± 0.1.98 (°C. days)/decade), especially after the observed climate shift in 2013. In the post-2013 period, there were rapidly increasing MHW trends in the North Sea, with a 64% increase in the frequency of events and a 24% increase in duration compared to the pre-2013 period. In contrast, the detrended approach indicated an insignificant trend in all MHW characteristics, suggesting that long-term SST warming was the main driver of the observed MHW increase in the North Sea. In addition, the trend-attribution ratio showed that the relative contribution of long-term SST warming to the observed trend in MHW occurrence in the North Sea was about 80%, while the rest was due to internal variability. These results confirmed that long-term SST trends, rather than SST variability trends, dominated the change in MHW in the North Sea. They also confirmed the linear relationship between mean SST and MHW and suggested that MHW occurrence in the North Sea will continue to increase under global warming.

A new SST record was set in the North Sea in May 2024. This SST record was associated with the strongest (2.2°C) and longest (27 days, from May 10 to June 5, 2024) MHW event. The main cause of this MHW event was the observed anomalous anticyclonic circulation over the Baltic Sea and southern Norway, which reduced cloud cover and wind speed and increased shortwave solar radiation over the North Sea. Finally, we investigated the complex relationship between MHW and surface chlorophyll-a concentrations in the North Sea. The results indicated contrasting responses of chlorophyll-a to MHW, with a decrease in the northeastern part of the North Sea and an increase in the southern North Sea, while the opposite was true during marine cold spells. Further research is needed to predict future MHW in the North Sea under different climate scenarios and to investigate the extreme compound events (e.g., marine, atmospheric heatwaves, and heavy rainfall) and their consequences and impacts in the North Sea.

https://doi.org/10.5194/egusphere-2025-1578
Preprint. Discussion started: 16 April 2025

Data Availability Statement: The original contributions presented in the study are included in the article; further inquiries can be directed to the corresponding author.

Conflicts of Interest: The authors declare that they have no conflicts of interest, except that the last co-author (Aida Alvera-Azcárate) is a member of the editorial board of Ocean Science.

Author Contributions: Conceptualization: BM, AB, DVDZ, and AAA. Methodology and visualization: BM, AAA, DVDZ, and AB. Writing –original draft preparation: BM. Review and editing: BM, AB, DVDZ, and AAA. Supervision: AAA. All authors have read and agreed to the published version of the manuscript.

Funding: This work was fully funded by the STEREO-IV (Support To Exploitation and Research in Earth Observation) program administered by BELSPO (Belgian Science Policy Office) through the North-Heat project (STEREO-IV BELSPO # project SR/00/404).

Acknowledgments: The authors would like to thank the organizations that provided the data used in this work, including the Copernicus Marine Environment Monitoring Service (CMEMS), the European Centre for Medium-Range Weather Forecasts (ECMWF), and the National Oceanic and Atmospheric Administration (NOAA).

References

Alheit, J., Gröger, J., Licandro, P., McQuinn, I. H., Pohlmann, T., and Tsikliras, A. C.: What happened in the mid-1990s? The coupled ocean-atmosphere processes behind climate-induced ecosystem changes in the Northeast Atlantic and the Mediterranean, Deep Sea Research Part II: Topical Studies in Oceanography, 159, 130–142, https://doi.org/10.1016/J.DSR2.2018.11.011, 2019.

Alvera-Azcárate, A., Van der Zande, D., Barth, A., Troupin, C., Martin, S., and Beckers, J. M.: Analysis of 23 Years of Daily Cloud-Free Chlorophyll and Suspended Particulate Matter in the Greater North Sea, Front Mar Sci, 8, 707632, https://doi.org/10.3389/FMARS.2021.707632/BIBTEX, 2021.

Amaya, D., Jacox, M. G., Fewings, M. R., Saba, V. S., Stuecker, M. F., Rykaczewski, R. R., Ross, A. C., Stock, C. A., Capotondi, A., Petrik, C. M., Bograd, S. J., Alexander, M. A., Cheng, W., Hermann, A. J., Kearney, K. A., and Powell, B. S.: Marine heatwaves need clear definitions so coastal communities can adapt, Nature 2023 616:7955, 616, 29–32, https://doi.org/10.1038/d41586-023-00924-2, 2023.

Amorim, F. de L. L. de, Balkoni, A., Sidorenko, V., and Wiltshire, K. H.: Analyses of sea surface chlorophyll a trends and variability from 1998 to 2020 in the German Bight (North Sea), Ocean Science, 20, 1247–1265, https://doi.org/10.5194/OS-20-1247-2024, 2024.

Berthou, S., Renshaw, R., Smyth, T., Tinker, J., Grist, J. P., Wihsgott, J. U., Jones, S., Inall, M., Nolan, G., Berx, B., Arnold, A., Blunn, L. P., Castillo, J. M., Cotterill, D., Daly, E., Dow, G., Gómez, B., Fraser-Leonhardt, V., Hirschi, J. J. M., Lewis, H. W., Mahmood, S., and Worsfold, M.: Exceptional atmospheric conditions in June 2023 generated a northwest European marine heatwave which contributed to breaking land temperature records, Communications Earth & Environment 2024 5:1, 5, 1–11, https://doi.org/10.1038/s43247-024-01413-8, 2024.

Biguino, B., Antunes, C., Lamas, L., Jenkins, L. J., Dias, J. M., Haigh, I. D., and Brito, A. C.: 40 years of changes in sea surface temperature along the Western Iberian Coast, Science of The Total Environment, 888, 164193, https://doi.org/10.1016/j.scitotenv.2023.164193, 2023.

Capotondi, A., Rodrigues, R. R., Sen Gupta, A., Benthuysen, J. A., Deser, C., Frölicher, T. L., Lovenduski, N. S., Amaya, D. J., Le Grix, N., Xu, T., Hermes, J., Holbrook, N. J., Martinez-Villalobos, C., Masina, S., Roxy, M. K., Schaeffer, A., Schlegel, R. W., Smith, K. E., and Wang, C.: A global overview of marine heatwaves in a changing climate, Communications Earth & Environment 2024 5:1, 5, 1–17, https://doi.org/10.1038/s43247-024-01806-9, 2024.

Chauhan, A., Smith, P. A. H., Rodrigues, F., Christensen, A., St. John, M., and Mariani, P.: Distribution and impacts of long-lasting marine heat waves on phytoplankton biomass, Front Mar Sci, 10, 1177571, https://doi.org/10.3389/FMARS.2023.1177571/BIBTEX, 2023.

https://doi.org/10.5194/egusphere-2025-1578
Preprint. Discussion started: 16 April 2025

Chen, W., Staneva, J., Grayek, S., Schulz-Stellenfleth, J., and Greinert, J.: The role of heat wave events in the occurrence and persistence of thermal stratification in the southern North Sea, Natural Hazards and Earth System Sciences, 22, 1683–1698, https://doi.org/10.5194/NHESS-22-1683-2022, 2022.

Cheng, L., Foster, G., Hausfather, Z., Trenberth, K. E., and Abraham, J.: Improved Quantification of the Rate of Ocean Warming, J Clim, 35, https://doi.org/10.1175/JCLI-D-21-0895.1, 2022.

Desmit, X., Nohe, A., Borges, A. V., Prins, T., De Cauwer, K., Lagring, R., Van der Zande, D., and Sabbe, K.: Changes in chlorophyll concentration and phenology in the North Sea in relation to de-eutrophication and sea surface warming, Limnol Oceanogr, 65, 828–847, https://doi.org/10.1002/LNO.11351, 2020.

Ducrotoy, J. P., Elliott, M., and De Jonge, V. N.: The North Sea, Mar Pollut Bull, 41, 5–23, https://doi.org/10.1016/S0025-326X(00)00099-0, 2000.

Frölicher, T. L. and Laufkötter, C.: Emerging risks from marine heat waves, Nature Communications 2018 9:1, 9, 1–4, https://doi.org/10.1038/s41467-018-03163-6, 2018.

Frölicher, T. L., Fischer, E. M., and Gruber, N.: Marine heatwaves under global warming, Nature 2018 560:7718, 560, 360–364, https://doi.org/10.1038/s41586-018-0383-9, 2018.

Greene, C. A., Thirumalai, K., Kearney, K. A., Delgado, J. M., Schwanghart, W., Wolfenbarger, N. S., Thyng, K. M., Gwyther, D. E., Gardner, A. S., and Blankenship, D. D.: The Climate Data Toolbox for MATLAB, Geochemistry, Geophysics, Geosystems, 20, 3774–3781, https://doi.org/10.1029/2019GC008392, 2019.

Hamed, K. H. and Ramachandra Rao, A.: A modified Mann-Kendall trend test for autocorrelated data, J Hydrol (Amst), 204, 182–196, https://doi.org/10.1016/S0022-1694(97)00125-X, 1998.

Harris, R. M. B., Beaumont, L. J., Vance, T. R., Tozer, C. R., Remenyi, T. A., Perkins-Kirkpatrick, S. E., Mitchell, P. J., Nicotra, A. B., McGregor, S., Andrew, N. R., Letnic, M., Kearney, M. R., Wernberg, T., Hutley, L. B., Chambers, L. E., Fletcher, M. S., Keatley, M. R., Woodward, C. A., Williamson, G., Duke, N. C., and Bowman, D. M. J. S.: Biological responses to the press and pulse of climate trends and extreme events, Nature Climate Change 2018 8:7, 8, 579–587, https://doi.org/10.1038/s41558-018-0187-9, 2018.

Hersbach, H., Bell, B., Berrisford, P., Hirahara, S., Horányi, A., Muñoz-Sabater, J., Nicolas, J., Peubey, C., Radu, R., Schepers, D., Simmons, A., Soci, C., Abdalla, S., Abellan, X., Balsamo, G., Bechtold, P., Biavati, G., Bidlot, J., Bonavita, M., De Chiara, G., Dahlgren, P., Dee, D., Diamantakis, M., Dragani, R., Flemming, J., Forbes, R., Fuentes, M., Geer, A., Haimberger, L., Healy, S., Hogan, R. J., Hólm, E., Janisková, M., Keeley, S., Laloyaux, P., Lopez, P., Lupu, C., Radnoti, G., de Rosnay, P., Rozum, I., Vamborg, F., Villaume, S., and Thépaut, J. N.: The ERA5 global reanalysis, Quarterly Journal of the Royal Meteorological Society, 146, 1999–2049, https://doi.org/10.1002/qj.3803, 2020.

Hobday, A. J., Alexander, L. V., Perkins, S. E., Smale, D. A., Straub, S. C., Oliver, E. C. J., Benthuysen, J. A., Burrows, M. T., Donat, M. G., Feng, M., Holbrook, N. J., Moore, P. J., Scannell, H. A., Sen Gupta, A., and Wernberg, T.: A hierarchical approach to defining marine heatwaves, Prog Oceanogr, 141, 227–238, https://doi.org/10.1016/j.pocean.2015.12.014, 2016.

Huang, B., Liu, C., Banzon, V., Freeman, E., Graham, G., Hankins, B., Smith, T., and Zhang, H. M.: Improvements of the Daily Optimum Interpolation Sea Surface Temperature (DOISST) Version 2.1, J Clim, 34, 2923–2939, https://doi.org/10.1175/JCLI-D-20-0166.1, 2021.

Hughes, S. L., Holliday, N. P., and Gaillard, F.: Variability in the ICES/NAFO region between 1950 and 2009: Observations from the ICES Report on Ocean Climate, ICES Journal of Marine Science, 69, 706–719, https://doi.org/10.1093/icesjms/fss044, 2012.

Jacobs, Z. L., Jebri, F., Wakelin, S., Strong, J., Popova, E., Srokosz, M., and Loveridge, A.: Marine heatwaves and cold spells in the Northeast Atlantic: what should the UK be prepared for?, Front Mar Sci, 11, 1434365, https://doi.org/10.3389/FMARS.2024.1434365/BIBTEX, 2024.

Jin, Z. F. and Zhang, W. Z.: Statistical Characteristics of Remote Sensing Extreme Temperature Anomaly Events in the Taiwan Strait, Remote Sensing 2024, Vol. 16, Page 3091, 16, 3091, https://doi.org/10.3390/RS16163091, 2024.

https://doi.org/10.5194/egusphere-2025-1578
Preprint. Discussion started: 16 April 2025

Kirby, R. R., Beaugrand, G., Lindley, J. A., Richardson, A. J., Edwards, M., and Reid, P. C.: Climate effects and benthic–pelagic coupling in the North Sea, Mar Ecol Prog Ser, 330, 31–38, https://doi.org/10.3354/MEPS330031, 2007.

Lee, S., Park, M. S., Kwon, M., Park, Y. G., Kim, Y. H., and Choi, N.: Rapidly Changing East Asian Marine Heatwaves Under a Warming Climate, J Geophys Res Oceans, 128, e2023JC019761, https://doi.org/10.1029/2023JC019761, 2023.

Li, Y., Ren, G., Wang, Q., and Mu, L.: Changes in marine hot and cold extremes in the China Seas during 1982–2020, Weather Clim Extrem, 39, 100553, https://doi.org/10.1016/J.WACE.2023.100553, 2023.

Marin, M., Feng, M., Phillips, H. E., and Bindoff, N. L.: A Global, Multiproduct Analysis of Coastal Marine Heatwaves: Distribution, Characteristics, and Long-Term Trends, J Geophys Res Oceans, 126, e2020JC016708, https://doi.org/10.1029/2020JC016708, 2021.

Marzocchi, A., Hirschi, J. J. M., Holliday, N. P., Cunningham, S. A., Blaker, A. T., and Coward, A. C.: The North Atlantic subpolar circulation in an eddy-resolving global ocean model, Journal of Marine Systems, 142, 126–143, https://doi.org/10.1016/J.JMARSYS.2014.10.007, 2015.

Mohamed, B. and Skliris, N.: Recent sea level changes in the Red Sea: Thermosteric and halosteric contributions, and impacts of natural climate variability, Prog Oceanogr, 231, 103416, https://doi.org/10.1016/J.POCEAN.2025.103416, 2025.

Mohamed, B., Barth, A., and Alvera-Azcárate, A.: Extreme marine heatwaves and cold-spells events in the Southern North Sea: classifications, patterns, and trends, Front Mar Sci, 10, 1258117, https://doi.org/10.3389/FMARS.2023.1258117/BIBTEX, 2023.

Oliver, E. C. J.: Mean warming not variability drives marine heatwave trends, Climate Dynamics 2019 53:3, 53, 1653–1659, https://doi.org/10.1007/S00382-019-04707-2, 2019.

Pecuchet, L., Mohamed, B., Hayward, A., Alvera-Azcárate, A., Dörr, J., Filbee-Dexter, K., Kuletz, K. J., Luis, K., Manizza, M., Miller, C. E., U Staehr, P. A., Szymkowiak, M., Wernberg, T., Fauchald, P., Ma, J., Clement Kinney, J., and Pau, S.: Arctic and Subarctic marine heatwaves and their ecological impacts, Front Environ Sci, 13, 1473890, https://doi.org/10.3389/FENVS.2025.1473890, 2025.

Pettitt, A. N.: A Non-Parametric Approach to the Change-Point Problem, Appl Stat, 28, 126, https://doi.org/10.2307/2346729, 1979.

Rebstock, G. A.: Climatic regime shifts and decadal-scale variability in calanoid copepod populations off southern California, Glob Chang Biol, 8, 71–89, https://doi.org/10.1046/J.1365-2486.2002.00456.X, 2002.

Reynolds, R. W., Smith, T. M., Liu, C., Chelton, D. B., Casey, K. S., and Schlax, M. G.: Daily High-Resolution-Blended Analyses for Sea Surface Temperature, J Clim, 20, 5473–5496, https://doi.org/10.1175/2007JCLI1824.1, 2007.

Robson, J., Lohmann, K., Smith, D., and Palmer, M. D.: Causes of the Rapid Warming of the North Atlantic Ocean in the Mid-1990s, J Clim, 25, 4116–4134, https://doi.org/10.1175/JCLI-D-11-00443.1, 2012.

Rodionov, S. N.: A sequential algorithm for testing climate regime shifts, Geophys Res Lett, 31, https://doi.org/10.1029/2004GL019448, 2004.

Simon, A., Poppeschi, C., Plecha, S., Charria, G., and Russo, A.: Coastal and regional marine heatwaves and cold spells in the northeastern Atlantic, Ocean Science, 19, 1339–1355, https://doi.org/10.5194/OS-19-1339-2023, 2023a.

Simon, A., Pires, C., Frölicher, T. L., and Russo, A.: Long-term warming and interannual variability contributions' to marine heatwaves in the Mediterranean, Weather Clim Extrem, 42, 100619, https://doi.org/10.1016/J.WACE.2023.100619, 2023b.

Tinker, J. and Howes, E. L.: The impacts of climate change on temperature (air and sea), relevant to the coastal and marine environment around the UK, Marine Climate Change Impacts Partnership, 30 pp., https://doi.org/10.14465/2020.arc01.tem, 2020.

https://doi.org/10.5194/egusphere-2025-1578
Preprint. Discussion started: 16 April 2025

Villeneuve, A. R. and White, E. R.: Predicting organismal response to marine heatwaves using dynamic thermal tolerance landscape models, Journal of Animal Ecology, https://doi.org/10.1111/1365-2656.14120, 2024.

Wang, F., Shao, W., Yu, H., Kan, G., He, X., Zhang, D., Ren, M., and Wang, G.: Re-evaluation of the Power of the Mann-Kendall Test for Detecting Monotonic Trends in Hydrometeorological Time Series, Front Earth Sci (Lausanne), 8, 14, https://doi.org/10.3389/feart.2020.00014, 2020.

Xu, T., Newman, M., Capotondi, A., Stevenson, S., Di Lorenzo, E., and Alexander, M. A.: An increase in marine heatwaves without significant changes in surface ocean temperature variability, Nature Communications 2022 13:1, 13, 1–12, https://doi.org/10.1038/s41467-022-34934-x, 2022.

Zeileis, A., Kleiber, C., Walter, K., and Hornik, K.: Testing and dating of structural changes in practice, Comput Stat Data Anal, 44, 109–123, https://doi.org/10.1016/S0167-9473(03)00030-6, 2003.

Zhao, Z. and Marin, M.: A MATLAB toolbox to detect and analyze marine heatwaves, J Open Source Softw, 4, 1124, https://doi.org/10.21105/joss.01124, 2019.